GPCR Engineering Yields High-Resolution Structural Insights into β_2-Adrenergic Receptor Function

Daniel M. Rosenbaum, *et al.*

Science **318**, 1266 (2007);
DOI: 10.1126/science.1150609

This copy is for your personal, non-commercial use only.

If you wish to distribute this article to others, you can order high-quality copies for your colleagues, clients, or customers by clicking here.

Permission to republish or repurpose articles or portions of articles can be obtained by following the guidelines here.

The following resources related to this article are available online at www.sciencemag.org (this infomation is current as of November 21, 2011):

Updated information and services, including high-resolution figures, can be found in the online version of this article at:
http://www.sciencemag.org/content/318/5854/1266.full.html

Supporting Online Material can be found at:
http://www.sciencemag.org/content/suppl/2007/11/21/318.5854.1266.DC2.html
http://www.sciencemag.org/content/suppl/2007/10/23/1150609.DC1.html

A list of selected additional articles on the Science Web sites **related to this article** can be found at:
http://www.sciencemag.org/content/318/5854/1266.full.html#related

This article has been **cited by** 281 article(s) on the ISI Web of Science

This article has been **cited by** 80 articles hosted by HighWire Press; see:
http://www.sciencemag.org/content/318/5854/1266.full.html#related-urls

This article appears in the following **subject collections:**
Biochemistry
http://www.sciencemag.org/cgi/collection/biochem

Science (print ISSN 0036-8075; online ISSN 1095-9203) is published weekly, except the last week in December, by the American Association for the Advancement of Science, 1200 New York Avenue NW, Washington, DC 20005. Copyright 2007 by the American Association for the Advancement of Science; all rights reserved. The title *Science* is a registered trademark of AAAS.

GPCR Engineering Yields High-Resolution Structural Insights into β_2-Adrenergic Receptor Function

Daniel M. Rosenbaum,[1]* Vadim Cherezov,[2]* Michael A. Hanson,[2]
Søren G. F. Rasmussen,[1] Foon Sun Thian,[1] Tong Sun Kobilka,[1] Hee-Jung Choi,[1,3]
Xiao-Jie Yao,[1] William I. Weis,[1,3] Raymond C. Stevens,[2]† Brian K. Kobilka[1]†

AUTHORS' SUMMARY

Heterotrimeric guanine nucleotide–binding protein (G protein) coupled receptors (GPCRs) are a remarkably versatile family of transmembrane signaling molecules that present extraordinary therapeutic potential as drug targets for a wide spectrum of diseases (*1*). A better understanding of GPCR structure will help to elucidate the mechanism by which they transmit signals across the plasma membrane and will facilitate the development of more effective and selective drugs. Rhodopsin, the light-sensitive photoreceptor found in the mammalian eye, is also a GPCR, and its structure has been determined. Obtaining high-resolution structures of GPCRs other than rhodopsin, however, has been challenging because of their low natural abundance and inherent structural flexibility and instability (*2*). As a result, the application of structure-based drug discovery to GPCRs has largely been limited to the use of rhodopsin-based homology models. We have applied targeted protein engineering to make other GPCRs better candidates for crystallographic structure analysis, using the human β_2-adrenergic receptor as an initial candidate. The β_2-adrenergic receptor binds the hormones adrenaline and noradrenaline to regulate cardiovascular and pulmonary function. Our results show that targeted protein engineering can be used to obtain high-resolution structures of GPCRs.

Efforts to crystallize the wild-type (WT) β_2-adrenergic receptor have been unsuccessful. We identified the third intracellular loop (ICL3) as a possible contributor to the difficulties in crystallization. This region interacts with signaling molecules such as G proteins. ICL3 is poorly structured and contributes to the relatively unrestricted movement of the transmembrane helices, which leads to the receptor's conformational heterogeneity and crystallization problems. Truncation of ICL3 could reduce the movement of the helices, but this would also reduce the polar surface area that is important for forming crystal-lattice contacts. Thus, we replaced ICL3 with T4 lysozyme (T4L), a well-folded protein that adds a polar surface and simultaneously restricts the movement of transmembrane helices linked by the inserted sequence (see the figure). The resulting fusion protein could be efficiently expressed in insect cells and purified. It also retained ligand binding affinities near those of the WT receptor and could undergo conformational changes upon agonist binding.

The engineered protein formed crystals in two different lipid environments: bicelles and lipidic cubic phase. Crystals grown in lipidic cubic phase yielded a 2.4 Å x-ray diffraction data set from which we determined the structure by molecular replacement, using T4 lysozyme and a polyalanine model of the transmembrane regions of rhodopsin as search models [see (*3*)].

One must be concerned that the structural modifications that facilitated crystal formation could produce a high-resolution structure that does not reflect the WT β_2-adrenergic receptor. The fusion protein exhibited slightly elevated agonist binding affinities; however, antagonist binding affinities were normal, and only minor differences were observed when the β_2-adrenergic receptor–T4L structure was compared to a 3.4 Å structure of the WT β_2-adrenergic receptor crystallized in complex with an antibody fragment (*4*). Therefore, with the exception of ICL3, the structure of β_2-adrenergic receptor–T4L probably reflects that of the native receptor.

Although we know the structure of the GPCR rhodopsin, our structure of the β_2-adrenergic receptor now provides a high-resolution view of a GPCR that binds diffusible hormones and neurotransmitters and should facilitate structure-based drug development. Moreover, it can help to reveal how structural changes are propagated from the agonist binding site to the G protein–coupling domains. The methods that we used to obtain these crystals will probably be applicable to other GPCRs, allowing the determination of their structures and increasing our understanding of transmembrane signal transduction and drug discovery for this important class of molecules.

Nevertheless, a full understanding of the structural basis of GPCR activation will require a high-resolution structure of a complex between a receptor with an agonist bound and its G protein, as well as methods to assess the dynamics of their interaction that cannot be captured by the static snapshots provided by x-ray crystallography. Future nuclear magnetic resonance (NMR) experiments, which capture some of the dynamics, could identify key GPCR residues: those critical for binding different classes of ligands, propagating conformational changes, and forming allosteric interaction sites for signaling partners such as G proteins and arrestins. When interpreted in the context of high-resolution crystal structures, NMR and other dynamics experiments will lead to a better understanding of GPCR signaling and how such signaling can be manipulated with small molecules to therapeutic effect.

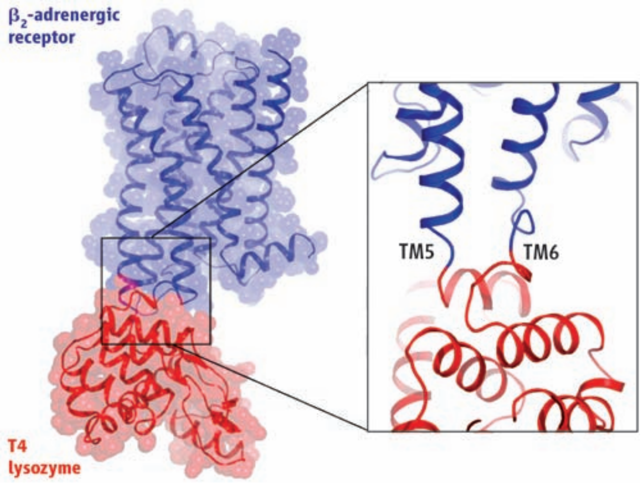

Replacement of an intracellular loop of the β_2-adrenergic receptor with lysozyme stabilized two flexible helices (5 and 6), allowing crystallization of the fusion protein and determination of the structure of this medically important membrane receptor.

Summary References

1. K. L. Pierce, R. T. Premont, R. J. Lefkowitz, *Nat. Rev. Mol. Cell Biol.* **3**, 639 (2002).
2. B. K. Kobilka, X. Deupi, *Trends Pharmacol. Sci.* **28**, 397 (2007).
3. V. Cherezov *et al., Science* **318**, 1258, (2007); published online 25 October 2007 (10.1126/science.1150577).
4. S. G. F. Rasmussen *et al., Nature*; published online 21 October 2007; 10.1038/nature06325.

FULL-LENGTH ARTICLE

The β_2-adrenergic receptor (β_2AR) is a well-studied prototype for heterotrimeric guanine nucleotide–binding protein (G protein)–coupled receptors (GPCRs) that respond to diffusible hormones and neurotransmitters. To overcome the structural flexibility of the β_2AR and to facilitate its crystallization, we engineered a β_2AR fusion protein in which T4 lysozyme (T4L) replaces most of the third intracellular loop of the GPCR ("β_2AR-T4L") and showed that this protein retains near-native pharmacologic properties. Analysis of adrenergic receptor ligand-binding mutants within the context of the reported high-resolution structure of β_2AR-T4L provides insights into inverse-agonist binding and the structural changes required to accommodate catecholamine agonists. Amino acids known to regulate receptor function are linked through packing interactions and a network of hydrogen bonds, suggesting a conformational pathway from the ligand-binding pocket to regions that interact with G proteins.

The adrenergic receptors make up a class of heterotrimeric guanine nucleotide–binding protein (G protein)–coupled receptors (GPCRs) that play a central role in mediating the effects of catecholamine hormones. In contrast to rhodopsin, which is expressed at very high levels in photoreceptor cells and has the ligand retinal covalently bound (*1*), other GPCRs such as the β_2-adrenergic receptor (β_2AR) generally express at low levels, bind diffusible ligands, and exhibit greater functional and structural plasticity (*2*). The β_2AR was the first non-rhodopsin GPCR to be cloned and has been one of the most extensively studied members of this large receptor family.

To obtain high-resolution structural information on the β_2AR, we increased its proteolytic stability and crystallizability by eliminating the C-terminal tail and replacing most of the third intracellular loop (ICL3) with the protein T4 lysozyme (T4L). The optimized β_2AR-T4L protein was crystallized in lipidic cubic phase, as described in the companion paper by Cherezov *et al.* (*3*), and the resulting 2.4 Å resolution crystal structure reveals the interface between the receptor and the ligand carazolol, a partial inverse agonist (*4*). Analysis of mutagenesis data in light of the structure clarifies the roles of different amino acids in inverse-agonist binding and implies that rearrangement of the binding pocket accompanies agonist binding. In addition, the structure reveals how mutations known to cause constitutive activity or uncoupling of agonist binding and G protein activation are distributed between the ligand-binding pocket and the cytoplasmic surface of the protein, such that changes in side chains due to interaction with the ligand can be transmitted through the structure to the site of G protein interaction.

β_2AR-T4L: A crystallizable GPCR fusion protein. The conformational complexity that makes GPCRs versatile signaling molecules may contribute to the difficulty of crystallizing these proteins (*2*). Despite substantial efforts, we were unable to grow diffraction-quality crystals from purified, homogeneous wild-type (WT) β_2AR. This was probably due to conformational variability of the flexible ICL3 and C terminus, as well as the relatively small polar surface available for crystal contacts. Fluorescence resonance energy transfer experiments show that the C-terminal portion of the β_2AR is in an extended conformation (*5*), a property that may be important for the role of this region in interacting with signaling and scaffold proteins, but one that would probably interfere with crystal-lattice formation. ICL3, which links the cytoplasmic ends of helices V and VI, is functionally important both for the specificity of receptor–G protein interactions and for G protein activation. In the β_2AR, this domain is susceptible to proteolysis; however, proteolytic cleavage does not lead to dissociation of the transmembrane segments linked by the ICL3. In fact, β_2AR helices I to V and helices VI and VII behave as independent folding domains that can be expressed on separate plasmids and assemble to form a functional "split" receptor (*6*). Therefore, we speculated that ICL3 links two domains with a relatively dynamic interface, which could be important for function but may also contribute to greater instability.

Because the majority of membrane protein crystals form through contacts of the nonmembranous portions of the molecule, we sought to improve the chances of β_2AR crystallization by replacing ICL3 with a well-structured, soluble domain that might aid in the formation of lattice contacts. The initial criteria for choosing the inserted soluble protein were that the N and C termini would approximate the predicted distance between the cytoplasmic ends of helix V and helix VI and that the protein would crystallize under a variety of conditions. T4L is a small, stable protein that fulfills these criteria (*7*). The N and C termini of WT T4L are 10.7 Å apart in Protein Data Bank (PDB) structure 2LZM (*8*), compared with a distance of 15.9 Å between the carbonyl carbon of residue $228^{5.63}$ (*9*) and the amide nitrogen of residue $241^{6.24}$ in the high-resolution structure of rhodopsin (PDB 1U19) (*10*).

DNA encoding the T4L protein (Cys^{54} → Thr^{54}, Cys^{97} → Ala^{97}) (*11*) was initially cloned into the human β_2AR gene, guided by a comparison of ICL3 length and sequence among class A GPCRs (*12*): residues $234^{5.73}$ to $259^{6.21}$ of the β_2AR were replaced by residues 2 to 164 of T4L (construct "E3" in Fig. 1A). In addition, the receptor was truncated at position 365, which aligns approximately with the position of the rhodopsin C terminus. Although these modifications resulted in a receptor that was expressed efficiently in Sf9 cells, further optimization was carried out to reduce the length of the junction between the receptor and the T4L termini (*13*). Several candidate constructs are illustrated in Fig. 1A, and selected immunofluorescence images of transfected, permeabilized human embryonic kidney (HEK) 293 cells are shown in Fig. 1B. Relative to the initial construct, we could remove three residues from the cytoplasmic end of helix V, three from the C-terminal end of T4L, and three from the N terminus of helix VI, all without losing substantial cell-surface expression. The final construct used for crystallization trials (β_2AR-T4L) has residues $231^{5.70}$ to $262^{6.24}$ of the β_2AR replaced by amino acids 2 to 161 of T4L (D1 in Fig. 1A). Similar reduction of flexibility through minimization of linker length has been important in previous crystallization studies on soluble fusion proteins (*14*).

Functional properties of β_2AR-T4L. We measured saturation binding of [^{3}H]DHA to the β_2AR-T4L, as well as competition binding of the inverse agonist ICI-118,551 and several agonists (Fig. 2A, fig. S1, and table S1). The results show that β_2AR-T4L has WT affinity for the antagonist [^{3}H]DHA and the inverse agonist ICI-118,551, whereas the affinity for both agonists (e.g., isoproterenol, epinephrine, formoterol) and a partial agonist (salbutamol) is two-to-threefold higher relative to WT β_2AR. Higher agonist binding affinity is a property associated with constitutively active mutants (CAMs) of GPCRs. CAMs of the β_2AR also exhibit elevated basal, agonist-independent activation of the stimulatory G protein for adenylyl cyclase (Gs) and typically have lower expression levels and reduced stability (*15*, *16*). β_2AR-T4L exhibits binding properties of a CAM, but it expresses at levels exceeding 1 mg/liter of Sf9 cell culture, is more resistant to trypsin proteolysis than the WT β_2AR (fig. S2), and retains binding activity in detergent at 37°C, as well as the WT receptor (fig. S3).

β_2AR-T4L did not couple to Gs, as expected, because of the replacement of ICL3 by T4L. To assess whether the fused protein alters receptor function at the level of its ability to undergo conformational changes, we used a covalently attached fluorescent probe as a reporter for ligand-induced structural changes. Fluorophores attached at Cys$265^{6.27}$, at the cytoplasmic end of helix VI, detect agonist-induced conformational changes that correlate with the efficacy of the agonist toward G protein activation (*17*–*20*). Detergent-

---

[1]Department of Molecular and Cellular Physiology, Stanford University School of Medicine, Stanford, CA 94305, USA. [2]Department of Molecular Biology, The Scripps Research Institute, La Jolla, CA 92037, USA. [3]Department of Structural Biology, Stanford University School of Medicine, Stanford, CA 94305, USA.

*These authors contributed equally to this work.

†To whom correspondence should be addressed. E-mail: stevens@scripps.edu (R.C.S.); kobilka@stanford.edu (B.K.K.)

solubilized β$_2$AR365 (WT receptor truncated at 365) and β$_2$AR-T4L were each labeled with monobromobimane, which has been used previously to monitor conformational changes of the β$_2$AR (*21*). The addition of the agonist isoproterenol to purified β$_2$AR365 induces a decrease in fluorescence intensity and a shift in the wavelength at maximum intensity (λ_{max}) for the attached bimane probe (Fig. 2B and table S2). These changes in intensity and λ_{max} are consistent with an agonist-induced increase in polarity around bimane. A smaller change is observed with the partial agonist salbutamol, whereas the inverse agonist ICI-118,551 had little effect. For the β$_2$AR-T4L, there are subtle differences in the baseline spectrum of the bimane-labeled fusion protein, as might be expected if the environment around Cys265$^{6.27}$ is altered by T4L. However, the full agonist isoproterenol induces a qualitatively similar decrease in intensity and rightward shift in λ_{max}. Thus, the presence of the fused T4L does not prevent agonist-induced conformational changes. The partial agonist salbutamol induced larger responses in β$_2$AR-T4L than were observed in WT β$_2$AR, and there was a small increase in fluorescence in response to the inverse agonist ICI-118,551. These properties are observed in CAMs (*15*, *22*) and are consistent with the higher affinities for agonists and partial agonists exhibited by β$_2$AR-T4L. Therefore, we conclude that the T4L fusion induces a partial constitutively active phenotype in the β$_2$AR, probably caused by changes at the cytoplasmic ends of helices V and VI.

Comparison between β$_2$AR-T4L and β$_2$AR-Fab structures. The β$_2$AR-T4L fusion strategy is validated by a comparison of its structure to that of WT β$_2$AR complexed with a Fab that recognizes a three-dimensional epitope consisting of the N- and C-terminal ends of ICL3, determined at an anisotropic resolution of 3.4 Å/3.7 Å (*23*). Figure 3A illustrates the similarity between the fusion and antibody complex approaches to β$_2$AR crystallization, in that both strategies rely on attachment (covalent or noncovalent, respectively) of a soluble protein partner between helices V and VI. A major difference between the two structures is that the extracellular loops and the carazolol ligand could not be modeled in the β$_2$AR-Fab complex, whereas these regions are resolved in the structure of β$_2$AR-T4L. Nonetheless, it is clear that the T4L insertion does not substantially alter the receptor. Superposition of the two structures (fig. S4) illustrates that the transmembrane helices of the receptor components are very similar (root mean square deviation = 0.8 Å for 154 common modeled transmembrane Cα positions versus 2.3 Å between β$_2$AR-T4L and the 154 equivalent residues in rhodopsin), especially when the modest resolution of the Fab complex is taken into account.

There is one major difference between the Fab-complex and chimeric-receptor structures that can be attributed to the presence of T4L. The cytoplasmic end of helix VI is pulled outward as a result of the fusion to the C terminus of T4L, which alters the packing of Phe264$^{6.26}$ at the end of helix VI (Fig. 3B). In the Fab-complex β$_2$AR, interactions between Phe264$^{6.26}$ and residues in helix V, helix VI, and ICL2 may be important in maintaining the β$_2$AR in the basal state. The loss of these packing interactions in β$_2$AR-T4L could contribute to the higher agonist binding affinity characteristic of a CAM.

An unexpected difference between the structure of rhodopsin and the β$_2$AR-T4L involves the sequence E/DRY (*24*) found at the cytoplasmic end of helix III in 71% of class A GPCRs. In rhodopsin, Glu134$^{3.49}$ and Arg135$^{3.50}$ form a network of hydrogen bond and ionic interactions with Glu247$^{6.30}$ at the cytoplasmic end of helix VI. These interactions have been referred to as an "ionic lock" that stabilizes the inactive state of rhodopsin and other class A members (*25*). However, the arrangement of the homologous residues is considerably different in β$_2$AR-T4L: Arg131$^{3.50}$ interacts primarily with Asp130$^{3.49}$

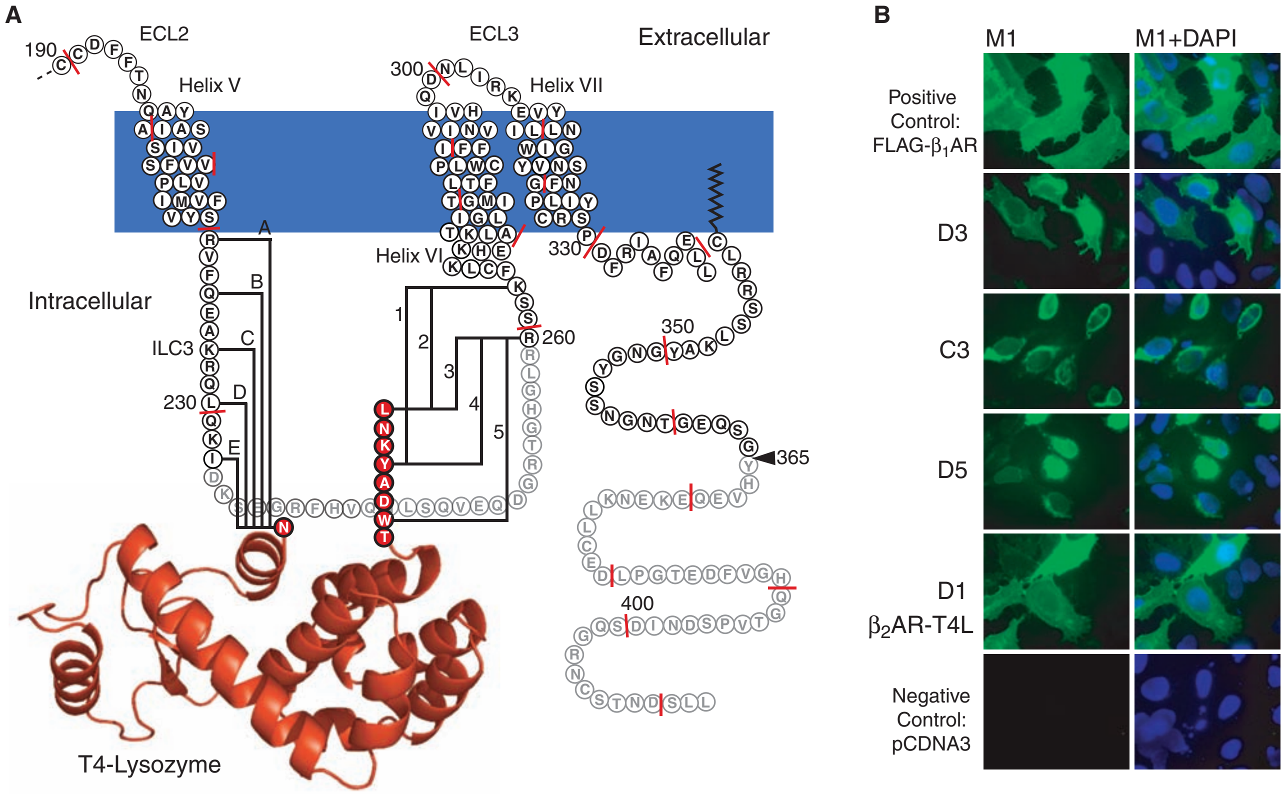

Fig. 1. Design and optimization of the β$_2$AR-T4L fusion protein. (**A**) The sequence of the region of the β$_2$AR targeted for insertion of a crystallizable domain is shown, and the positions of the junctions between the receptor and T4L (red) for various constructs are indicated. The sequences that were initially replaced or removed are faded. Red lines are shown after every tenth residue. ECL, extracellular loop. (**B**) Immunofluorescence images of HEK293 cells expressing selected fusion constructs. (Left) M1 anti-FLAG signal corresponding to antibody bound to the N terminus of the receptor. (Right) Same signal merged with blue emission from 4′,6′-diamidino-2-phenylindole (nuclear staining for all cells). Plasma membrane staining is observed in the positive control, D3, and D1, whereas C3 and D5 are retained in the endoplasmic reticulum.

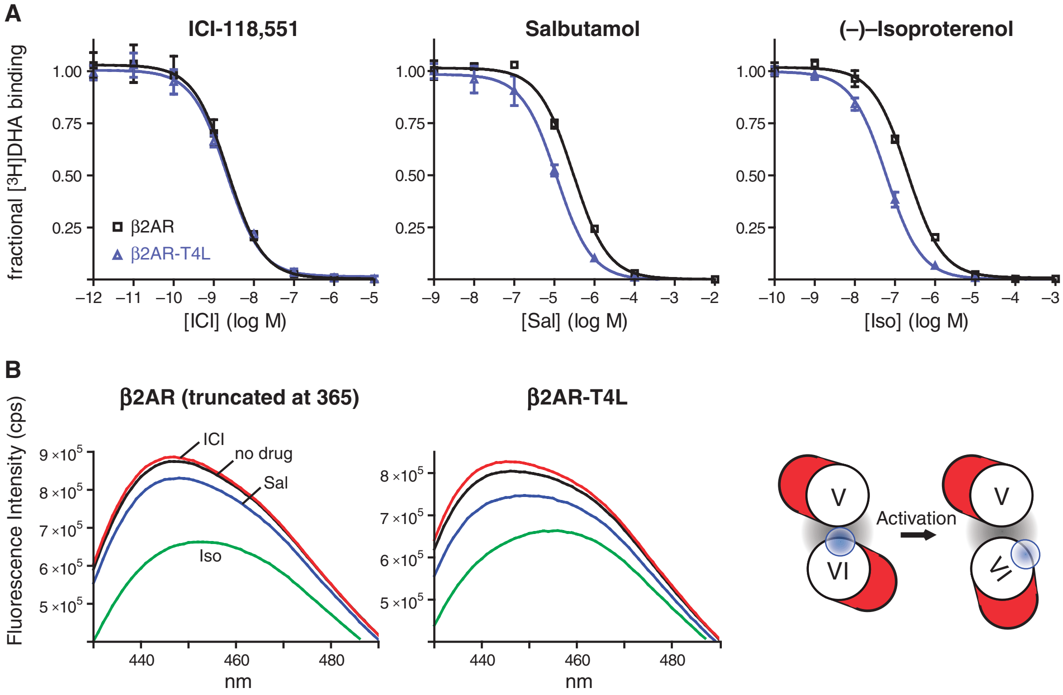

Fig. 2. Functional characterization of β_2AR-T4L. (**A**) Affinity competition curves for adrenergic ligands binding to β_2AR-T4L and WT β_2AR. Binding experiments on membranes isolated from Sf9 insect cells expressing the receptors were performed as described (*13*). (**B**) β_2AR-T4L is still able to undergo ligand-induced conformational changes. Bimane fluorescence spectra (excitation at 350 nm) of detergent-solubilized β_2AR-T4L and WT β_2AR truncated at 365, labeled under conditions that selectively modify Cys265$^{6.27}$ (*13*), were measured after incubating the unliganded receptors with compounds for 15 min at room temperature. The cartoon illustrates that the observed changes in fluorescence can be interpreted as a movement of the bimane probe from a more buried, hydrophobic environment to a more polar, solvent-exposed position. cps, counts per second.

and a sulfate ion rather than with Glu268$^{6.30}$, and the distance between helix III and helix VI is greater than in rhodopsin (Fig. 3C). This difference might be explained by the interaction between Glu268$^{6.30}$ and Arg8 of T4L; however, the arrangement of Asp130$^{3.49}$ and Arg131$^{3.50}$ and the distance between helix III and helix VI is very similar to that observed in the β_2AR-Fab structure. Although the presence of an antibody or T4L at the ICL3 region could potentially affect the arrangement of these residues, the fact that similar ionic-lock structures were obtained using two different approaches suggests that a broken ionic lock may be a genuine feature of the carazolol-bound state of the receptor.

Ligand binding to the β_2AR. The β_2AR-T4L fusion protein was purified and crystallized in complex with the inverse agonist carazolol. Carazolol stabilizes the β_2AR against extremes of pH and temperature, perhaps related to its unusually high binding affinity (equilibrium dissociation constant $K_d < 0.1$ nM) and slow dissociation kinetics (half-time $t_{1/2} \sim 30$ hours) (fig. S5). The interactions between carazolol and β_2AR-T4L are depicted schematically in Fig. 4. The carbazole ring system is oriented roughly perpendicular to the plane of the membrane, and the alkylamine chain (atoms 15 to 22 in the model) is nearly parallel to the heterocycle (Fig. 5, A and B). Carazolol was modeled into the electron density (*3*) as the (S)-(–) isomer because of the higher affinity of this enantiomer, despite the fact that a racemic mixture of the ligand was used in crystallization. Asp113$^{3.32}$, Tyr316$^{7.43}$, and Asn312$^{7.39}$ present a constellation of polar functional groups to the alkylamine and alcohol moieties of the ligand, with the Asp113$^{3.32}$ and Asn312$^{7.39}$ side chains forming close contacts (<3 Å) with the

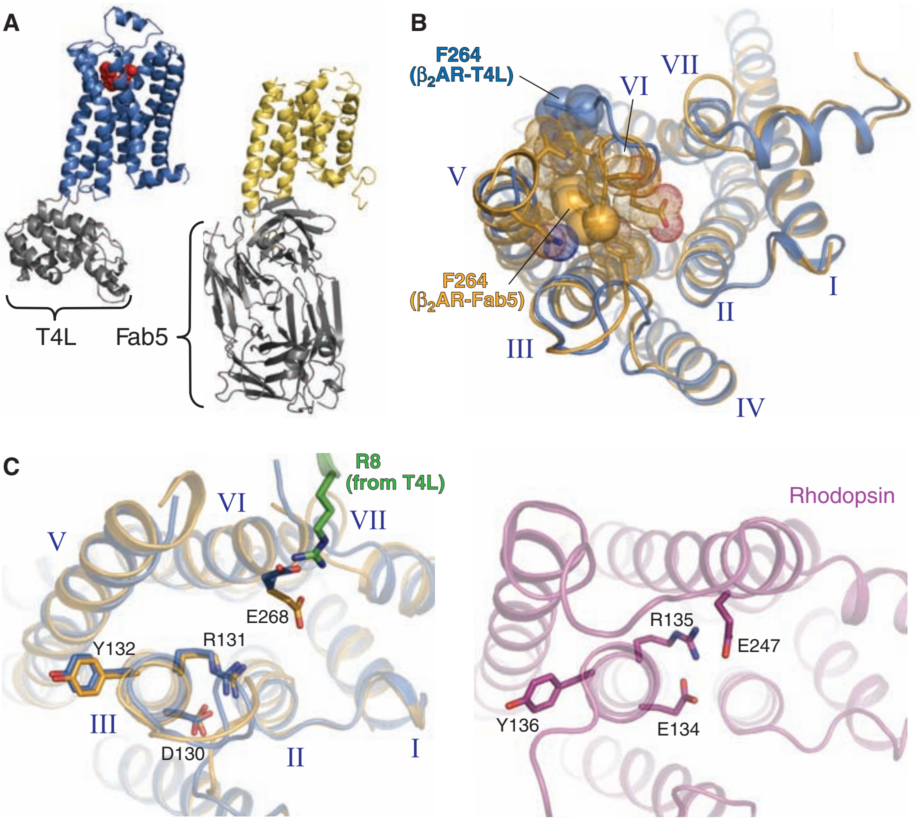

Fig. 3. (**A**) Side-by-side comparison of the crystal structures of the β_2AR-T4L fusion protein and the complex between β_2AR365 and a Fab fragment. The receptor component of the fusion protein is shown in blue (with modeled carazolol as red spheres), whereas the receptor bound to Fab5 is yellow. (**B**) Differences in the environment surrounding Phe264$^{6.26}$ (shown as spheres) for the two proteins. (**C**) Analogous interactions to the ionic lock between the E(D)RY motif and Glu247$^{6.30}$ seen in rhodopsin (right panel, purple) are broken in both structures of the β_2AR (left panel, blue and yellow as above). PyMOL (*43*) was used for the preparation of all figures.

O_{17} and N_{19} atoms of carazolol (Figs. 4 and 5, A and B). Asp113$^{3.32}$ was one of the first β_2AR residues shown to be important for ligand binding; the D113N mutation causes a complete loss of detectable affinity for antagonists (*26*) and a decrease in the potency of agonists toward cell-based G protein activation by over four orders of magnitude (*27*). Likewise, mutations of Asn312$^{7.39}$ perturb β_2AR binding to agonists and antagonists: Changes to nonpolar amino acids (Ala or Phe) reduce affinities to undetectable levels, whereas retention of a polar functionality (Thr or Gln) gives partial affinity (*28*). On the opposite end of the ligand near helix V, N_7 of the carbazole heterocycle forms a hydrogen bond with the side-chain hydroxyl of Ser203$^{5.42}$. Mutations of Ser203$^{5.42}$ specifically decrease β_2AR affinity toward catecholamine agonists and aryloxyalkylamine ligands with nitrogen-containing heterocycles such as pindolol (*29*) and, by implication, carazolol. Thus, the polar interactions between carazolol and the receptor observed in the crystal structure agree with the known biochemical data. The contribution of Tyr316$^{7.43}$ to antagonist and

Fig. 4. Schematic representation of the interactions between β_2AR-T4L and carazolol at the ligand binding pocket. The residues shown here have at least one atom within 4 Å of the ligand in the 2.4 Å resolution crystal structure.

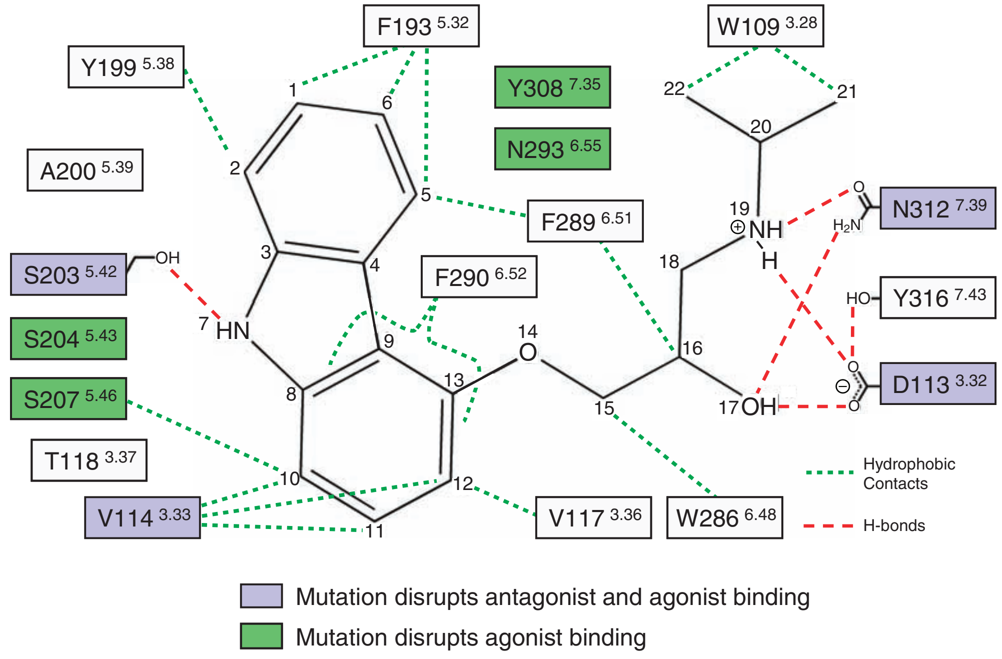
F193 5.32
W109 3.28
Y199 5.38
Y308 7.35
N293 6.55
A200 5.39
F289 6.51
N312 7.39
S203 5.42
F290 6.52
Y316 7.43
S204 5.43
S207 5.46
D113 3.32
T118 3.37
V114 3.33
V117 3.36
W286 6.48
OH
HN
NH
H
H2N
O
HO
OH
1
2
3
4
5
6
7
8
9
10
11
12
13
14
15
16
17
18
19
20
21
22
Hydrophobic Contacts
H-bonds
Mutation disrupts antagonist and agonist binding
Mutation disrupts agonist binding

Fig. 5. Ligand binding pocket of β_2AR-T4L with carazolol bound. (**A**) Residues within 4 Å of the ligand are shown as sticks, with the exception of A200, N293, F289, and Y308. Residues that form polar contacts with the ligand (distance cutoff: 3.5 Å) are shown in green, other residues are gray, and carazolol is yellow (in all panels, oxygens are red and nitrogens are blue). (**B**) Same as (A), except that the ligand is oriented with its amine facing out of the page. W109 is not shown. (**C**) Packing interactions between carazolol and all residues within 5 Å of the ligand. The view is from the extracellular side of the membrane. Carazolol is shown as yellow spheres, and receptor residues are shown as sticks within van der Waals dot surfaces. Val114$^{3.33}$, Phe193$^{5.32}$, and Phe290$^{6.52}$ are red, and all other residues are gray. (**D**) Model of (–)-isoproterenol (magenta sticks) in the ligand binding pocket observed in the crystal structure. A model of the agonist with optimal bond lengths and angles was obtained from the PRODRG server (*44*), and the dihedral angles were adjusted to the values observed in the homologous atoms of bound carazolol (16 to 22 in Fig. 4). The one remaining unaccounted dihedral in (–)-isoproterenol was adjusted in order to place the catechol ring in the same plane as the C_{16}–C_{15}–O_{14} plane in carazolol. Residues known to specifically interact with agonists are shown as green sticks.

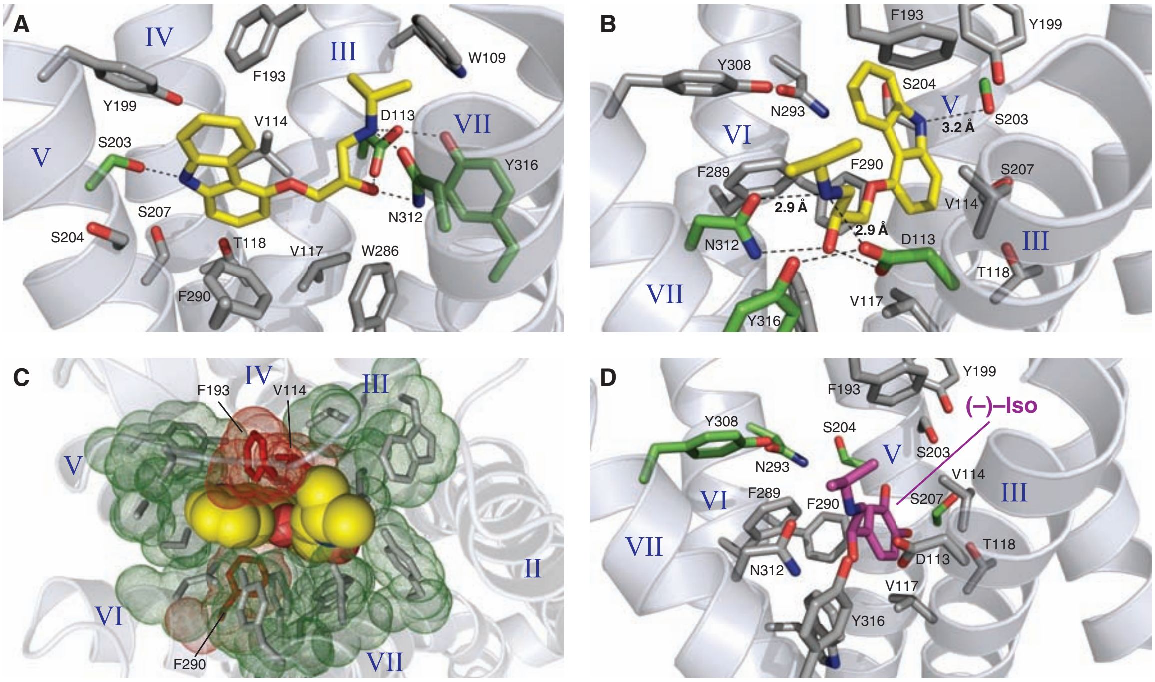
A
IV
III
W109
F193
Y199
V114
D113
VII
V
S203
Y316
S207
N312
S204
T118
V117
W286
F290
B
F193
Y199
Y308
S204
N293
V
VI
3.2 Å
S203
F289
F290
S207
2.9 Å
2.9 Å
V114
N312
D113
III
T118
VII
V117
Y316
C
IV
F193
V114
III
V
II
VI
F290
VII
D
Y199
F193
(–)-Iso
Y308
S204
V
S203
N293
V114
VI
F289
F290
S207
III
VII
T118
N312
D113
V117
Y316

agonist affinity remains to be tested; this residue is conserved as Tyr in all sequenced adrenergic receptor genes (*12*).

Figure 5C shows the tight packing between carazolol and surrounding amino acids that buries 790 Å^2 of surface area from solvent; specific contacts are depicted schematically in Fig. 4. Notable among the hydrophobic residues contacting carazolol are Val114$^{3.33}$, Phe290$^{6.52}$, and Phe193$^{5.32}$. The side chain of Val114$^{3.33}$ from helix III makes multiple contacts with the C_8-to-C_{13} ring of the carbazole heterocycle, and Phe290$^{6.52}$ from helix VI forms an edge-to-face aromatic interaction with the same ring. As a result, these two amino acids form a hydrophobic "sandwich" with the portion of the aryl moiety that is common to many adrenergic antagonists. The mutation of Val114$^{3.33}$ to Ala was shown to decrease β$_2$AR affinity toward the antagonist alprenolol by one order of magnitude, as well as to lower affinity for the agonist epinephrine 300-fold (*30*). Phe193$^{5.32}$ is different from other carazolol contact residues in that it is located on the second extracellular loop, in the path of hormone accessibility to the binding pocket. This amino acid contributes more buried surface area than any other residue to the interface between β$_2$AR-T4L and carazolol (table S3). Therefore, Phe193$^{5.32}$ is likely to contribute substantially to the energy of β$_2$AR-carazolol complex formation, and the position of this residue on the extracellular side of the binding site may allow it to act as a gate that contributes to the unusually slow dissociation of the ligand (fig. S5).

Analysis of the binding pocket provides insights into the structural basis for pharmacologic selectivity between the β$_2$AR and closely related adrenergic receptors such as the β$_1$AR. The affinities of these two receptors for certain ligands, such as ICI-118,551, betaxolol, and RO363 (*31*), differ by up to 100-fold. Curiously, all of the amino acids in the carazolol binding pocket are conserved between the β$_1$AR and β$_2$AR [fig. S6 in (*13*)]. The majority of the 94 amino acid differences between the β$_1$AR and β$_2$AR are found in the cytoplasmic and extracellular loops. Whereas residues that differ in the transmembrane segments generally face the lipid bilayer, eight residues lie at the interface between helices and may influence helix packing. The structural basis for pharmacologic differences between β$_1$AR and β$_2$AR must, therefore, arise from amino acid differences in the entrance to the binding pocket or subtle differences in the packing of helices. Evidence for the latter comes from chimeric-receptor studies (*32*) in which successive exchange of helices between β$_1$AR and β$_2$ARs led to a gradual change in affinity for the β$_2$AR selective ICI-118,551 and the β$_1$AR selective betaxolol.

As discussed above, β$_2$AR-T4L shows CAM-like properties with respect to agonist binding affinities, suggesting that the unliganded β$_2$AR-T4L may exist in a more active conformation than the WT β$_2$AR. Nevertheless, as shown in Fig. 2B, β$_2$AR-T4L can be stabilized in an inactive conformation by an inverse agonist. Because β$_2$AR-T4L was crystallized with bound carazolol, a partial inverse agonist, the structure most likely represents an inactive state. This is consistent with the similarity of the β$_2$AR-T4L and β$_2$AR-Fab5 carazolol-bound structures. To assess whether conformational changes are required to accommodate catecholamines, a model

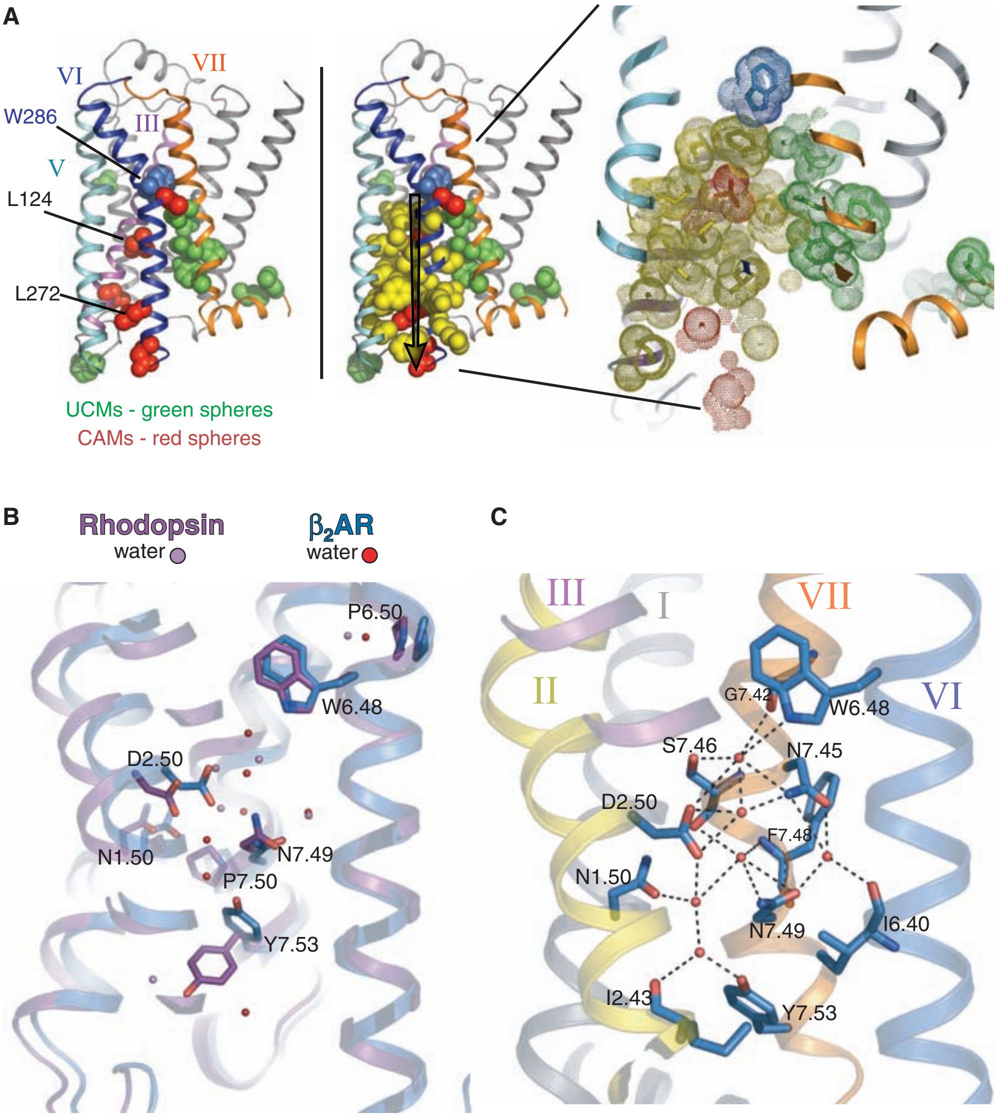

Fig. 6. Packing interactions in the β$_2$AR that are likely to be modulated during the activation process. (**A**) (Left) Residues previously demonstrated to be CAMs (*16*, *25*, *37*–*39*, *45*) or UCMs (*26*, *41*, *46*–*49*) are shown as van der Waals spheres mapped onto a backbone cartoon of the β$_2$AR-T4L structure. (Right) Residues that are found within 4 Å of the CAMs Leu124$^{3.43}$ and Leu272$^{6.34}$ are shown as yellow spheres or dot surfaces. A vertical cross section through the structure illustrates that these surrounding residues connect the CAMs on helices III and VI with the UCMs on helix VII through packing interactions. (**B**) In both β$_2$AR-T4L (blue) and rhodopsin (purple), a network of ordered water molecules is found at the interface between the transmembrane helices at their cytoplasmic ends. (**C**) Network of hydrogen bonding interactions between water molecules and β$_2$AR-T4L residues (side chains shown as blue sticks), notably three UCMs on helix VII (orange) and one on helix II (yellow). In (B) and (C), only Ballesteros-Weinstein numbers (9) are used to identify amino acids.

of isoproterenol was placed in the binding site such that common atoms (16 to 22 in Fig. 4) were superimposed onto the analogous carazolol coordinates in the crystal structure (Fig. 5D). Residues Ser204$^{5.43}$ and Ser207$^{5.46}$ are critical for catecholamine binding and activation of the β$_2$AR, with Ser204$^{5.43}$ hydrogen bonding to the meta-hydroxyl and Ser207$^{5.46}$ to the para-hydroxyl of the catechol ring, respectively (*33*). In our model, the catechol hydroxyls of isoproterenol face the appropriate Ser residues on helix V, but the distances are too long for hydrogen bonding (6.8 Å from the meta-hydroxyl oxygen to the side-chain oxygen of Ser204$^{5.43}$ and 4.8 Å from the para-hydroxyl oxygen to the side-chain oxygen of Ser207$^{5.46}$). In addition, Asn293$^{6.55}$ and Tyr308$^{7.35}$, two residues expected to form selective interactions with agonists based on the literature (*34*, *35*), are too distant to form productive polar or hydrophobic contacts with the modeled isoproteronol molecule. These observations suggest that agonist binding requires changes in the binding site relative to the carazolol-bound structure, unless common structural components of agonists and inverse agonists bind in a considerably different manner.

Structural insights into β$_2$AR activation. Biophysical studies provide evidence that conformational changes associated with activation of the β$_2$AR are similar to those observed for rhodopsin (*2*, *18*, *21*, *36*). Yet the highly efficient process of light activation of rhodopsin through the cis-trans isomerization of covalently bound retinal is very different from activation of the β$_2$AR and other GPCRs by diffusible hormones and neurotransmitters (*2*). Despite representing a static picture of the inverse agonist–bound state, the crystal structure of β$_2$AR-T4L may still provide clues as to how agonist binding is translated into structural changes in the cytoplasmic domains of receptor. Agonist binding occurs at the extracellular ends of helices III, IV, V, and VII, and G protein activation is mediated by the cytoplasmic ends. Whereas the structure is open at the extracellular face to form the ligand binding pocket, the helices are more closely packed in the intracellular half of the receptor. This close packing implies that isolated rigid-body movement of any of these helices is unlikely and that conformational changes can be accomplished only by rearrangement of the side chains forming the network of interactions between the helices. Biophysical studies show that structurally different agonists stabilize distinct active states (*17*, *20*), suggesting that different ligands could stabilize different combinations of side-chain rearrangements.

Analysis of mutations that affect β$_2$AR function provides insights into structural rearrangements that are likely to occur during receptor activation. Figure 6A illustrates the location of amino acids for which mutations lead to elevated basal, agonist-independent activity (CAMs), as well as amino acids for which mutations impair agonist activation [uncoupling mutations (UCMs)]. Residues for which CAMs have been described are likely to be involved in interactions that maintain the receptor in the inactive conformation. These amino acids are centrally located on helices III and VI. In contrast, positions in which UCMs have been observed are likely to form intramolecular interactions that stabilize the active state. A cluster of UCMs is found at the cytoplasmic end of helix VII. Neither CAMs nor UCMs are directly involved in agonist binding. Although the CAMs and UCMs are not directly connected in sequence, it is evident from the structure that they are linked through packing interactions, so that movements in one will probably affect the packing of others. For example, Fig. 6A (right panel) shows all amino acids with atoms within 4 Å of the two centrally located CAMs, Leu124$^{3.43}$ (*37*) and Leu272$^{6.34}$ (*38*). Several amino acids that pack against these CAMs also interact with one or more UCMs. Trp286$^{6.48}$ lies at the base of the binding pocket. It has been proposed that agonist binding leads to a change in the rotameric state of Trp286$^{6.48}$, with subsequent changes in the angle of the helical kink formed by Pro288$^{6.50}$ (*39*). It is likely that an agonist-induced change in the rotameric state of Trp286$^{6.48}$ will be linked to changes in side chains of CAMs and UCMs through packing interactions and propagated to the cytoplasmic ends of the helices and the associated intracellular loops that interact with G proteins and other signaling molecules.

In the structures of both rhodopsin and the β$_2$AR, a cluster of water molecules lies near the most highly conserved class A GPCR residues (Fig. 6B). It has been proposed that these water molecules may play a role in the structural changes involved in receptor activation (*40*). Figure 6C shows the network of potential hydrogen bonding interactions that link Trp286$^{6.48}$ with conserved amino acids extending to the cytoplasmic ends of helices. UCMs have been identified for four amino acids linked by this network: Asp79$^{2.50}$, Asn318$^{7.45}$, Asn322$^{7.49}$, and Y326$^{7.53}$ (*41*). This relatively loose-packed, water filled region is probably important in allowing conformational transitions, as there will be fewer steric restraints to side-chain repacking. Future structures of the agonist-bound state of the β$_2$AR will help to clarify the precise rearrangements that accompany activation of the receptor.

Although crystallization of β$_2$AR-T4L in the presence of other ligands remains an exciting prospect, future efforts to obtain structures of the catecholamine-bound receptor will be challenging because of the relatively low affinity of these compounds in the absence of G protein and their chemical lability. Moreover, biophysical studies indicate that agonist binding and activation is a multistep process involving distinct conformational intermediates (*2*, *17*, *19*–*21*, *42*), which produces structural heterogeneity even at saturating concentrations of agonist. It is therefore possible that structural elucidation of the active state of the β$_2$AR will be possible only through crystallization of the complex between agonist, β$_2$AR, and Gs.

References and Notes

1. H. G. Khorana, *J. Biol. Chem.* **267**, 1 (1992).
2. B. K. Kobilka, X. Deupi, *Trends Pharmacol. Sci.* **28**, 397 (2007).
3. V. Cherezov *et al.*, *Science* **318**, 1258 (2007); published online 25 October 2007 (10.1126/science.1150577).
4. The efficacy of a ligand describes the effect of the ligand on the functional properties of a GPCR. Agonists are defined as ligands that fully activate the receptor, partial agonists induce submaximal activation even at saturating concentrations, and inverse agonists inhibit basal receptor activity. Antagonists have no effect on basal activity but competitively block access of other ligands. Carazolol is defined as a partial inverse agonist because it suppresses only 50% of the basal activity of the β$_2$AR.
5. S. Granier *et al.*, *J. Biol. Chem.* **282**, 13895 (2007).
6. B. K. Kobilka *et al.*, *Science* **240**, 1310 (1988).
7. X. J. Zhang, J. A. Wozniak, B. W. Matthews, *J. Mol. Biol.* **250**, 527 (1995).
8. L. H. Weaver, B. W. Matthews, *J. Mol. Biol.* **193**, 189 (1987).
9. Ballesteros-Weinstein numbering is used throughout the text as superscripts to the protein numbering. Within each helix is a single, most conserved residue among the class A GPCRs. This residue is designated x.50, where x is the number of the transmembrane helix. All other residues on that helix are numbered relative to this conserved position.
10. T. Okada *et al.*, *J. Mol. Biol.* **342**, 571 (2004).
11. M. Matsumura, W. J. Becktel, M. Levitt, B. W. Matthews, *Proc. Natl. Acad. Sci. U.S.A.* **86**, 6562 (1989).
12. F. Horn *et al.*, *Nucleic Acids Res.* **31**, 294 (2003).
13. Materials and methods and supplementary figures are available as supporting material on *Science* Online.
14. D. R. Smyth, M. K. Mrozkiewicz, W. J. McGrath, P. Listwan, B. Kobe, *Protein Sci.* **12**, 1313 (2003).
15. U. Gether *et al.*, *J. Biol. Chem.* **272**, 2587 (1997).
16. S. G. Rasmussen *et al.*, *Mol. Pharmacol.* **56**, 175 (1999).
17. P. Ghanouni *et al.*, *J. Biol. Chem.* **276**, 24433 (2001).
18. P. Ghanouni, J. J. Steenhuis, D. L. Farrens, B. K. Kobilka, *Proc. Natl. Acad. Sci. U.S.A.* **98**, 5997 (2001).
19. G. Swaminath *et al.*, *J. Biol. Chem.* **279**, 686 (2004).
20. G. Swaminath *et al.*, *J. Biol. Chem.* **280**, 22165 (2005).
21. X. Yao *et al.*, *Nat. Chem. Biol.* **2**, 417 (2006).
22. P. Samama, S. Cotecchia, T. Costa, R. J. Lefkowitz, *J. Biol. Chem.* **268**, 4625 (1993).
23. S. G. F. Rasmussen *et al.*, *Nature*, published online 21 October 2007; 10.1038/nature06325.
24. Single-letter abbreviations for the amino acid residues are as follows: A, Ala; C, Cys; D, Asp; E, Glu; F, Phe; G, Gly; H, His; I, Ile; K, Lys; L, Leu; M, Met; N, Asn; P, Pro; Q, Gln; R, Arg; S, Ser; T, Thr; V, Val; W, Trp; and Y, Tyr.
25. J. A. Ballesteros *et al.*, *J. Biol. Chem.* **276**, 29171 (2001).
26. C. D. Strader *et al.*, *Proc. Natl. Acad. Sci. U.S.A.* **84**, 4384 (1987).
27. C. D. Strader *et al.*, *J. Biol. Chem.* **263**, 10267 (1988).
28. S. Suryanarayana, B. K. Kobilka, *Mol. Pharmacol.* **44**, 111 (1993).
29. G. Liapakis *et al.*, *J. Biol. Chem.* **275**, 37779 (2000).
30. P. Chelikani *et al.*, *Proc. Natl. Acad. Sci. U.S.A.* **104**, 7027 (2007).
31. Y. Sugimoto *et al.*, *J. Pharmacol. Exp. Ther.* **301**, 51 (2002).
32. T. Frielle, K. W. Daniel, M. G. Caron, R. J. Lefkowitz, *Proc. Natl. Acad. Sci. U.S.A.* **85**, 9494 (1988).
33. C. D. Strader, M. R. Candelore, W. S. Hill, I. S. Sigal, R. A. Dixon, *J. Biol. Chem.* **264**, 13572 (1989).
34. K. Wieland, H. M. Zuurmond, C. Krasel, A. P. Ijzerman, M. J. Lohse, *Proc. Natl. Acad. Sci. U.S.A.* **93**, 9276 (1996).
35. H. Kikkawa, M. Isogaya, T. Nagao, H. Kurose, *Mol. Pharmacol.* **53**, 128 (1998).
36. U. Gether *et al.*, *EMBO J.* **16**, 6737 (1997).
37. Y. X. Tao, A. N. Abell, X. Liu, K. Nakamura, D. L. Segaloff, *Mol. Endocrinol.* **14**, 1272 (2000).
38. A. D. Jensen *et al.*, *J. Biol. Chem.* **276**, 9279 (2001).
39. L. Shi *et al.*, *J. Biol. Chem.* **277**, 40989 (2002).
40. L. Pardo, X. Deupi, N. Dolker, M. L. Lopez-Rodriguez, M. Campillo, *ChemBioChem* **8**, 19 (2007).
41. L. S. Barak, L. Menard, S. S. Ferguson, A. M. Colapietro, M. G. Caron, *Biochemistry* **34**, 15407 (1995).
42. M. J. Lohse, C. Hoffmann, V. O. Nikolaev, J. P. Vilardaga, M. Bunemann, *Adv. Protein Chem.* **74**, 167 (2007).
43. W. L. DeLano, The PyMOL Molecular Graphics System (DeLano Scientific, Palo Alto, CA, 2002), www.pymol.org.
44. A. W. Schüttelkopf, D. M. F. van Aalten, *Acta Crystallogr. D Biol. Crystallogr.* **D60**, 1355 (2004).

45. M. J. Zuscik, J. E. Porter, R. Gaivin, D. M. Perez, *J. Biol. Chem.* **273**, 3401 (1998).
46. F. Z. Chung, C. D. Wang, P. C. Potter, J. C. Venter, C. M. Fraser, *J. Biol. Chem.* **263**, 4052 (1988).
47. O. Moro, M. S. Shockley, J. Lameh, W. Sadee, *J. Biol. Chem.* **269**, 6651 (1994).
48. S. A. Green, G. Cole, M. Jacinto, M. Innis, S. B. Liggett, *J. Biol. Chem.* **268**, 23116 (1993).
49. A. M. Gabilondo *et al.*, *Proc. Natl. Acad. Sci. U.S.A.* **94**, 12285 (1997).

50. B.K.K. managed the protein design, production, and purification. R.C.S. managed lipidic cubic phase (LCP)–based crystallization and data collection methods development and experiments. D.M.R. designed, engineered, and characterized the β_2AR-T4L fusion protein; supplied protein materials for all crystallization trials; grew and collected data from the bicelle crystals; collected, processed, and refined the 3.5 Å LCP structure; refined the 2.4 Å structure; analyzed the results; and wrote the initial draft of the manuscript. V.C. developed methods for and performed LCP crystallization, LCP crystal mounting, LCP data collection, model refinement, analyzed the results, and was involved in manuscript preparation. M.A.H. designed the blind crystal screening protocol, collected the 2.4 Å data set, processed the 2.4 Å data, solved the structure by molecular replacement at 3.5 Å and 2.4 Å resolution, and was involved in manuscript preparation. S.G.F.R. assisted with β_2AR-T4L characterization and purification, as well as manuscript preparation. F.S.T. expressed β_2AR-T4L in insect cells and, together with T.S.K., performed the initial stage of β_2AR purification. H.-J.C. assisted with the refinement and comparison with the β_2AR-Fab5 structure. X.-J.Y. developed the bimane fluorescence assay. W.I.W. assisted with low-resolution data collection and processing, solved the β_2AR-T4L molecular replacement problem at 3.5 Å, supervised the 2.4 Å refinement process, and participated in structure analysis and manuscript preparation. R.C.S. additionally assisted with β_2AR-T4L crystallization, 2.4 Å data collection, structure solution, refinement, structure analysis, and manuscript preparation. B.K.K. additionally assisted with the design of the β_2AR-T4L fusion strategy, β_2AR-T4L purification, β_2AR-T4L 3.5 Å synchrotron data collection, structure analysis, and manuscript preparation. The authors thank G. Schertler for help with initial diffraction experiments on LCP crystals performed at ID-13 at the European Synchrotron Radiation Facility and P. Day for help with cell culture and immunofluorescence experiments. The use of T4L insertions in membrane proteins has also been reported by Privé and co-workers for lactose permease. This work was supported by NIH grant F32 GM082028 (to D.M.R.); the Lundbeck Foundation (to S.G.F.R); NIH Roadmap Initiative grant P50 GM073197 and Protein Structure Initiative P50 GM62411 (to R.C.S.); National Institute of Neurological Disorders and Stroke grant NS028471, the Mather Charitable Foundations, Lundbeck, and the NIH Roadmap Initiative grant R21 GM075811 (to B.K.K.). H.-J.C. and W.I.W. were supported in part by NIH grant R01 GM056169. Coordinates and structure factors for β_2AR-T4L have been deposited in the Protein Data Bank with identification code 2RH1.

Supporting Online Material

www.sciencemag.org/cgi/content/full/1150609/DC1
Materials and Methods
Figs. S1 to S6
Tables S1 to S3
References

17 September 2007; accepted 11 October 2007
Published online 25 October 2007;
10.1126/science.1150609
Include this information when citing this paper.

Superconducting Pair Correlations in an Amorphous Insulating Nanohoneycomb Film

M. D. Stewart Jr.,[1] Aijun Yin,[2] J. M. Xu,[1,2] James M. Valles Jr.[1]*

The Cooper pairing mechanism that binds single electrons to form pairs in metals allows electrons to circumvent the exclusion principle and condense into a single superconducting or zero-resistance state. We present results from an amorphous bismuth film system patterned with a nanohoneycomb array of holes, which undergoes a thickness-tuned insulator-superconductor transition. The insulating films exhibit activated resistances and magnetoresistance oscillations dictated by the superconducting flux quantum $h/2e$. This $2e$ period is direct evidence indicating that Cooper pairing is also responsible for electrically insulating behavior.

The 50-year-old Bardeen Cooper Schrieffer (BCS) theory (*1*) provides a microscopic description of superconductivity in metals that also generally applies to superfluidity in other systems of fermions, including liquid ^{3}He (*2*) and ultracold atomic gases (*3*). BCS theory introduced a novel phase of matter consisting of weakly bound Cooper pairs of conduction electrons that condense into a single quantum state. This phase exhibits zero dc resistance because correlations among the Cooper pairs inhibit the scattering processes normally responsible for electrical dissipation (*1*). Counterintuitively, Cooper pair formation has also been invoked to account for recently uncovered high-resistance states of matter (*4*–*8*). Moreover, these states appear in amorphous ultrathin films (*5*, *7*–*9*), where the factors favoring insulating behavior can compete with Cooper pair formation (*10*).

The question of whether Cooper pairing occurs in systems with a resistive ground state is at the heart of discussions of the insulator–to-superconductor quantum phase transition (IST). Numerous systems, including ultrathin amorphous films (*11*) and wires (*12*) and high-temperature superconducting oxides (*8*), can be tuned from an insulating phase, which has a resistance that asymptotically approaches infinity in the zero temperature limit, to a superconducting phase, which has zero resistance. The tuning parameters, which include film thickness (*11*), magnetic field (*6*), and magnetic impurities (*13*), determine the quantum ground state of the system. Consequently, the transformation is deemed a quantum, rather than a thermal, phase transition (*4*). Models of ISTs broadly separate into those that do or do not presume that Cooper pairs exist in the insulating phase. If Cooper pairs are present, then models include only Bose degrees of freedom and Cooper pairs and vortices, and the IST occurs through Bose condensation (*4*). If not, then the microscopic interactions among the fermionic degrees of freedom, electrons, must be considered, and the very formation of pairs can dominate the IST (*14*). Intermediate models of bosons within a dissipative background of fermions have also been developed (*15*). However, opinions differ widely on which scenario applies for amorphous film systems, because some experiments support a boson-only picture and others do not. Electron tunneling measurements suggest that Cooper pairs first appear at the same thickness as superconductivity in thin elemental films, in support of fermionic models (*16*). On the other hand, signatures in the magnetoresistance of other amorphous films suggest that vortices (*17*) and/or Cooper pairs (*5*–*7*) can persist well into an insulating phase.

We have studied a set of films that undergo an IST and can be probed directly for Cooper pairs in their insulating phase. Our films consist of an ultrathin amorphous metal patterned with a nanometer honeycomb (NHC) array of holes, which are tuned to pass from an insulating to a superconducting state by increasing their thickness. The resistive phases of systems that also exhibit a superconducting phase have been scrutinized for Cooper pairs using Nernst-effect measurements of vortex motion (*18*), electron tunneling measurements of the density of states (*16*), and ac conductivity measurements (*19*). These reveal at least the presence of pairing fluctuations. It is desirable, however, to devise a detection scheme that is sensitive to the spatial phase coherence of the pair wavefunction and thus to long-lived Cooper pairs. We constructed a simple but effective platform, which relies on the magnetic field dependence of the pair wavefunction phase

---

[1] Department of Physics, Brown University, 182 Hope Street, Providence, RI 02912, USA. [2] Division of Engineering, Brown University, 182 Hope Street, Providence, RI 02912, USA.

*To whom correspondence should be addressed. E-mail: valles@physics.brown.edu